# Wavelength Selectable Solid-State Raman lasers in the Visible and Ultraviolet Ranges

**(Invited paper)**

**R. P. Mildren**

**Center for Lasers and Applications, Macquarie University, NSW, 2109, Australia**
**rmildren@ics.mq.edu.au**

**Abstract: Solid-state Raman lasers are known as important sources at normally difficult to access wavelengths, and our recent studies have shown that they also form the basis of a class of wavelength selectable lasers. This paper summarizes our recent studies in wavelength selectable Raman lasers in the visible (532-650 nm) and ultraviolet (266-321 nm).**

**Keywords:** Raman lasers, solid-state lasers, nonlinear optics, tunable, potassium gadolinium tungstate

## I. INTRODUCTION

In comparison to gases and liquids, solid-state Raman media feature high gain and improved thermal characteristics thereby allowing compact wavelength converters at substantial output powers. The Raman shift is typically 700-1100cm$^{-1}$, which is ideal for shifting to wavelengths such as in the yellow and UV-B (285-315nm) spectral regions that are not easily accessed by direct laser transitions. In contrast to other wavelength conversion schemes such as optical parametric oscillators, the Raman process is automatically phase-matched and as a result the conversion efficiency is not limited by the usual nonlinear phase-matching constraints such as angle and temperature acceptance.

In the past decade, several high-gain Raman materials such as potassium gadolinium or yttrium tungstate, barium nitrate and other tungstates have become available with good quality through suppliers in Russia, Europe and most recently China. The materials are robust and are relatively inexpensive for pieces as large as 10cm long. Research activity using these materials in Raman lasers has been steadily increasing and is detailed in several recently published reviews [1]-[4]. The Raman group at the Centre for Lasers and Applications and has been studying the use of such materials in a diverse range Raman laser devices. Mid-IR, visible and UV sources have been developed with output powers up to several watts in cw and pulsed output formats, while conversion efficiencies approaching the quantum efficiency (~90%) have been observed [5]. In addition to accessing normally difficult spectral regions, Raman lasers can also be configured to provide discrete tuning amongst a broad choice of output wavelengths.

## II. PRINCIPLES OF WAVELENGTH SELECTION

Raman lasers often employ a resonator in order to both lower the threshold for the nonlinear conversion process and as method to control the output spectrum according to the spectral characteristics of the resonator mirrors. A Raman resonator also enables generation of multiple intracavity fields (fundamental, first Stokes, second Stokes etc) with high intracavity power density. The inclusion of a nonlinear medium capable of sum or frequency generation of the various fundamental and Stokes combinations forms the basis for the wavelength selectability. Ammann [5] first reported Raman wavelength selection in 1979 using lithium iodate as the Raman medium, but the concept has only been developed more recently with the increased availability of high quality Raman materials and advances in diode pumped solid-state lasers. Selectability stems from the dynamic interactions between the fundamental and Stokes optical fields, as shown schematically in Fig. 1 where the output wavelength is determined by the phase-matching conditions in the sum frequency medium. Clearly, second harmonic generation of the fundamental proceeds efficiently provided the waves are phase-matched in the nonlinear medium and that the nonlinear coupling coefficient is larger than that for the Raman process. In the absence of second harmonic generation of the fundamental beam, however, the growth in the fundamental field and subsequent conversion into Stokes orders occurs rapidly in the high-Q resonator. For a single Raman mode of energy $h\mu_1$ (where $h$ is Planck's constant), the output Stokes spectrum consists of the equally spaced lines:

$$\nu_i = \nu_f - i\mu_1$$

where i is a non-negative integer and vf is the fundamental (ie., pump) frequency. With the generation of first Stokes in the resonator, wavelengths at either the second harmonic (SH) of the first Stokes or the sum frequency (SF) with fundamental can be selected. Under conditions of optimum efficiency, the SF or SH coupling coefficient is higher than the Raman process to ensure that energy is not lost by unwanted generation of higher Stokes orders.

The possible sum frequency and second harmonic frequencies available are $\nu_i + \nu_j$. For up to $n_m$ Stokes orders, there are $2n_m$ possible unique SF/SH wavelengths available since each additional Stokes order provides an additional second-harmonic wavelength and a unique

wavelength by sum frequency generation with the next lowest order. It is shown in Sec 5 that the number of output wavelength options increases markedly for a Raman material that provides gain on 2 Raman modes.

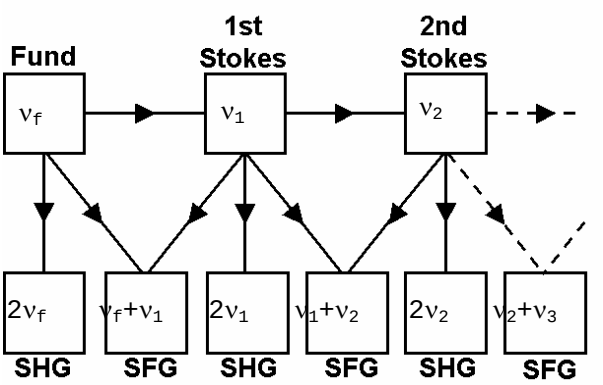


**Fig. 1** Schematic depiction of energy flow in a cascaded Raman laser with sum frequency material.

In this paper, results are presented for wavelength-selectable Raman lasers driven by a Nd:YAG fundamental beam generating output in the green/yellow/orange/red and UV-B (285-315nm) spectral regions. First, a Raman laser is described that demonstrates the key design and performance features for a visible system generating selectable output across several lines spanning the green-to-red. Our recent work in the development of UV solid-state 'Raman converters', consisting of an end-pumped Raman laser add-on to a standard pump laser, is then also described.

## III. SELECTABLE KGW RAMAN LASER IN THE GREEN-TO-RED

Efficient and powerful sources in the yellow-orange spectral region are in demand for applications in biomedicine and defence. Ammann's [6] work was based on an arclamp-pumped Nd:YALO and the Raman material $LiIO_3$, which also acted as a sum frequency mixing and second harmonic generation medium, to generate five wavelengths in the range 540-655 nm at output powers up to 600 mW. Potassium gadolinium tungstate (ie., $KGd(WO_4)_2$ or written herein as KGW) has emerged as excellent Raman material owing to its good thermophysical properties and high Raman gain [7]. Using KGW and a second sum frequency material (lithium triborate) enabled to separately optimise the two nonlinear processes [8].

### *A. Experimental details*

The layout of the intracavity Raman resonator is shown in Fig. 2. The laser resonator is typically 25 cm long and is defined by the coated face of the Nd:YAG laser crystal, the plane dichroic mirror at 45 degrees and an end mirror with radius of curvature 200 mm. The dichroic mirror has high reflectivity at 1064 nm and 1159 nm, and high transmission in the visible. The end mirror is a high reflector at the visible and infrared wavelengths. In the present case, high resonator losses for wavelengths >1250 nm (due to increased losses at AR coated surfaces and through the end mirrors) limits the second-order Stokes field and precludes higher-order (>2) Stokes generation. As a result, most efficient conversion is demonstrated for the sum frequencies of the second harmonics of the fundamental and first two Stokes orders.

The Nd:YAG is pumped with a fibre-coupled, 808 nm diode laser which produces 23 W output from a 400 µm diameter fibre (NA~0.22). The output from the end of the fibre is collimated and focused into a Nd:YAG laser crystal (5 mm diameter x 5 mm long, 1% doping) giving a pump spot size (beam radius) of approximately 300 microns. The pumped face of the Nd:YAG crystal is coated for high reflectivity at 1064 nm and 1159 nm and the second surface is anti-reflection coated for the near-infrared. The laser was acousto-optically Q-switched at 16 kHz repetition rate. The KGW crystal of dimensions 5 mm x 5 mm x 50 mm and was broadband anti-reflection coated for 1064-1150nm. The crystal was cut for propagation along the optical-axis (ie., $N_p$ axis) and oriented with optical $N_m$-axis vertical (which is parallel to the fundamental field) in order to select the 768cm$^{-1}$ Raman mode.

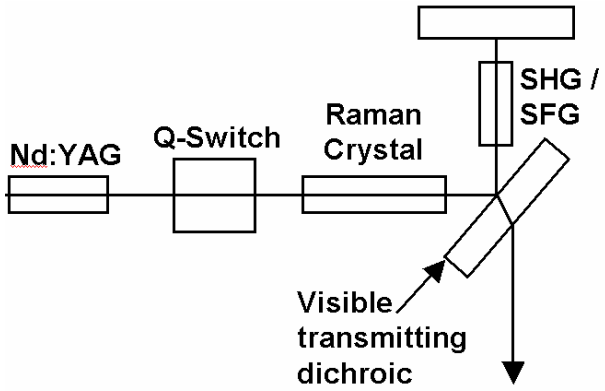


**Fig. 2** Experimental arrangement of the wavelength-selectable intracavity Raman laser.

Nonlinear crystals which are often used for SH or SF generation in this wavelength range include LBO, BBO, KTP and quasi-phase matched crystals. In this work, we selected LBO because it can be easily configured by either angle or temperature tuning in addition to its well known efficient conversion by SHG/SFG. LBO also enables excellent alignment stability in the case of the temperature tuned laser as non-critical phase matching occurs near room temperature.

### *B. Results*

For angle tuning, a single 4 mm x 4 mm x 10 mm piece of LBO cut for type-I non-critical phase matching (ie., $\theta$=90°, $\phi$=0°), and anti-reflection coated for the 1064 nm fundamental, was placed in the resonator cavity on a rotatable temperature-controlled mounting. Table I summarises laser performance for the LBO at 54°C (corresponding to non-critical phase matching at 579 nm at normal incidence). For 23 W of incident diode pump power (which corresponds to ~20W absorbed pump power), 1.8 W was obtained at 579 nm corresponding to 8% diode-to-yellow optical conversion efficiency. With the diode pump laser operating and the crystal tilted by approximately 10° (external angle), 0.95 W output power was generated at 555 nm (SFG of fundamental and first Stokes). Increasing the angle to 17° generated 1.7 W at 532 nm (second harmonic of the fundamental). Note that

changing the angle of the LBO crystal, results in some minor beam displacement that often makes it necessary to readjust the laser end-mirror in the horizontal plane. (However, mechanical arrangements providing automatic walk-off compensation could eliminate the need to realign the cavity end-mirror when wavelength switching by angle tuning.) As discussed in more detail below, generation of longer wavelengths corresponding to frequency mixtures of higher order Stokes fields (606 nm, 636 nm etc.) can be achieved by decreasing the LBO temperature or selecting other nonlinear materials.

**Table I** Output wavelength and output power versus LBO rotation angle.

| LBO Angle | Wavelength (nm) | Output Power (W) |
|---|---|---|
| 0° | 579 | 1.8 |
| 11° | 555 | 0.95 |
| 17° | 532 | 1.7 |

For temperature tuning, the strong dependence of wavelength on phase-matching temperature provided by LBO enables the output wavelength to be simply switched between 555 nm, 579 nm and 606 nm by varying the nonlinear crystal temperature over a fairly modest temperature range (<100°C) at fixed angle. As discussed in more detail below, phase matching can also be achieved for 532 nm by increasing its temperature to ~150°C, however, the extended temperature range is not practical for the Peltier thermo-electric heating and cooling needed in these experiments. Instead, two closely spaced intracavity LBO crystals (LBO1 and LBO2) were used to overcome this limitation and to also provide rapid (< 1 min) wavelength switching across the four wavelengths (532 nm, 555 nm, 579 nm and 606 nm) with only modest temperature changes (<50°C). The second LBO crystal (LBO2) was the same as LBO1 but cut for SHG from 1064 nm at 25C ($\phi$~11.5°). The temperature settings and output powers obtained are shown Table II.

**Table II** Temperature selection of output wavelength.

| Temp LBO1 | Temp LBO2 | Wavelength (nm) | Output Power (W) |
|---|---|---|---|
| 19°C | 52°C | 606 | 0.25 |
| 48°C | 52°C | 579 | 0.57 |
| 95°C | 52°C | 555 | 0.52 |
| - | 25°C | 532 | 1.5 |

Output power 1.5 W at 532 nm was achieved by adjusting the temperature of LBO2 to 25°C. Note that the temperature setting of LBO1 is not important under these conditions because efficient frequency doubling depletes the fundamental in preference to conversion to the first-Stokes. Switching to 555 nm was achieved by adjusting the temperature of LBO1 to 95°C, the phase-matching temperature for SFG of 1064 nm and 1159 nm, and by detuning the temperature of the LBO2 crystal (by heating to 52°C). The strong fundamental field now drives the first Stokes field in the resonator. SFG of 1064 nm and 1159 nm in LBO1 provides maximum 555 nm output obtained of 0.52 W. Similarly, with the LBO1 temperature set for phase matching at 579 nm (ie., ~48°C), we obtained 0.6 W at 3% diode-to-yellow conversion efficiency and with the LBO1 temperature set for SFG of the first and second Stokes (1159 nm + 1272 nm, 19°C), ~0.25 W output power was obtained at 606 nm.

In comparison to the results obtained using a single LBO crystal arrangement, the lower output powers are attributed to the additional insertion loss of the second LBO crystal and the effect of the additional resonator length on the pump-resonator mode overlap in the Nd:YAG rod. At 606 nm, the output power is low compared to the shorter wavelengths due to the aforementioned coating losses at 1272 nm. With improved mirror and AR coatings, substantial powers are anticipated at 606 nm and for wavelengths based on SHG and SFG of high Stokes orders.

A number of options are available which provide tuning over a large number of wavelengths. It is desirable in angle tuning to use small rotation angles as large angles introduce large reflection losses and also require larger aperture (and thus larger volume and more expensive) crystals. Whereas angle tuning has been demonstrated for three wavelengths for the LBO at 54ºC, using a lower LBO temperature would enable four or more wavelengths to be scanned for a similar range of angles. By using BBO as the nonlinear medium, the four wavelengths can be accessed within a 3.5° rotation. The smaller angle would enable switchability between more wavelengths for a narrow aperture crystal and avoids the high losses incurred for high incident angles.

Temperature tuning of a NCPM crystal offers an approach with the key practical advantages of excellent alignment stability, no mechanical movement of optics (which is desirable from the viewpoint of commercial systems), and the crystal can be fixed normal to the resonator axis where the insertion losses are minimised. Using a larger temperature range than investigated here (using a multi-stage Peltier cooler or a wire-wound heater for examples), it is possible to scan more than four wavelengths with a single LBO crystal, eg.,, 532 nm, 555 nm, 579 nm and 606 nm for the temperature range 17 - 145°C.

## IV. WAVELENGTH SELECTABLE ULTRAVIOLET RAMAN CONVERTERS

Few ultraviolet (UV) lasers sources exist at wavelengths between the 3rd and 4th harmonics of Nd lasers (265-350 nm), a spectral region where there is emerging demand in biohazard detection, environmental sensing and defence. Cerium doped fluoride lasers [9] and AlGaN semiconductor diodes [10] are presently receiving substantial interest owing to their significant practical advantages over frequency-doubled dye lasers and optical parametric oscillators. There is a need, however, for robust narrow-band sources with a broad tuning range.

While direct nonlinear frequency conversion of visible (eg., yellow) Raman lasers provide a straightforward

**Table III** UV wavelength, output energy and efficiency obtained at 10 Hz.

| Output Wavelength (nm) | Wavelength Assignment* | Max Energy (μJ) | Max Efficiency (%) | End-Mirror Reflectance (%) | Dichroc Reflectance (%) |
|---|---|---|---|---|---|
| 266.0 | SHG F | 136 | 5.8 | >99 | 98.5 |
| 272.6 | SFG F + S1 | 104 | 1.4 | >99 | >99 |
| 279.4 | SHG S1 | 223 | 2.4 | >99 | >99 |
| 286.7 | SFG S1 + S2 | 96 | 1.1 | >99 | >99 |
| 294.4 | SHG S2 | 164 | 1.6 | >99 | >99 |
| 302.3 | SFG S2 + S3 | 108 | 1.1 | >99 | >99 |
| 310.8 | SHG S3 | 88 | 1.1 | 71.5 | 98 |
| 319.7 | SFG S3 + S4 | 7.7 | 0.1 | 29 | 95 |

*Note that UV output may be derived by SFG of Stokes wavelengths separated by two or more orders, however, the corresponding phase matching angles are slightly displaced from the angle at which maximum output is obtained.

method of generating UV output near 290nm [11], the wavelength selectable advantages are gained by placing the sum frequency / second harmonic medium intracavity.

Here we summarize the performance of solid-state UV Raman lasers pumped at 532 nm that utilize intracavity Raman and intracavity sum-frequency mixing to generate wavelength-switchable UV output at wavelengths that span the entire UV-B as well as extending into the UV-A and UV-C. We have characterized the laser performance for a two pump lasers, one pumped at 10 Hz in order to investigate generation of high output pulses energies [8]. As demanded by many applications in biological and environmental sensing, we have also demonstrated performance at average powers up to 50 mW at kilohertz pulse rates.

### *A. Experimental details*

The Raman laser consisted of a KGW Raman crystal and beta-barium borate (BBO) nonlinear mixing medium positioned in a confocal resonator as shown in Fig. 3. The input coupler is highly transmissive (~90%T) at 532 nm and highly reflective for the first three Stokes orders (HR 559-660 nm). The KGW crystal (5 mm x 5 mm x 50mm), was AR coated for 532-600 nm and oriented in order to access the highest gain Stokes shift at 901cm$^{-1}$ (ie., laser propagation along the Ng crystallo-optic axis and the pump polarization parallel to Nm). The second harmonic or sum frequencies of the intracavity Stokes and fundamental fields was coupled from the resonator using a UV reflecting dichroic mirror placed between the BBO crystal (dimensions 4x4x7 mm, cut angle 44°) and the Raman crystal. This method of output coupling ensures that generated UV does not impinge on the KGW crystal, which has poor transmission for λ<350 nm.

Both pump lasers used were frequency-doubled, electro-optic Q-switched, Nd:YAG lasers of pulse duration typically 10ns full width half maximum. The 10 Hz pump laser was a commercial flash lamp pumped system (Lumonics, HyperYag) and the 5 kHz system was an air-cooled diode-pumped laser. Imaging optics were used to provide good overlap between the pump and Raman laser modes in the Raman crystal (~500mm @ 10 Hz and ~75mm at 5 kHz). At 10 Hz, the input beam diameter was ~0.5mm and the radius of curvature of the input coupler and end-mirrors were 100 cm and 200 cm respectively. For the 5 kHz pump source, the pump laser was focussed into the resonator using 100mm lens and the curvatures of the input coupler and end-mirror were 20 cm and 30 cm respectively.

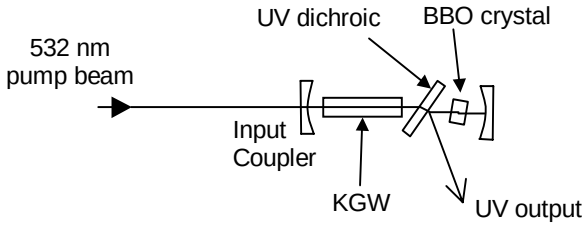


**Fig. 3** Schematic diagram of the UV Raman laser.

The UV output pulses were separated from residual visible output using a Pellin-Broca prism. The pump powers and resulting calculated efficiencies are based on the measured pump power incident on the input mirror.

### *B. Performance*

The output wavelength was selected by rotating the BBO nonlinear mixing crystal in the horizontal plane. Though a change in wavelength can easily be achieved without realignment of the end-mirror, alignment was re-optimized upon each wavelength change in order to generate maximum output. For the 10 Hz pump laser, the UV output for each of the 8 wavelengths varied with input pulse energy as shown in Fig. 4. The pulse energy at the second-harmonic of the pump wavelength (266 nm) increased to 130 μJ at more than 5% conversion efficiency but saturates for higher input energy. The saturation coincides with the onset of significant Stokes generation, indicating that the 266 nm output is limited by pump depletion from the competing Raman process.

Rotating the angle of the BBO crystal by ~3º (in the direction that decreases the subtended angle between the beam and optical axes) steps the output wavelength 273 nm, corresponding to the sum-frequency of the fundamental and the first Stokes. As with many of the UV wavelengths, the threshold is approximately 1-2 mJ, the output pulse energy increases monotonically over the investigated range of input energy, and the slope efficiency diminishes for input pulse energies > 4 mJ. The peak 273 nm conversion efficiency obtained was 1.35% from 4.5 mJ input energy, while the maximum output pulse energy achieved was 104 μJ at conversion efficiency

0.75%.

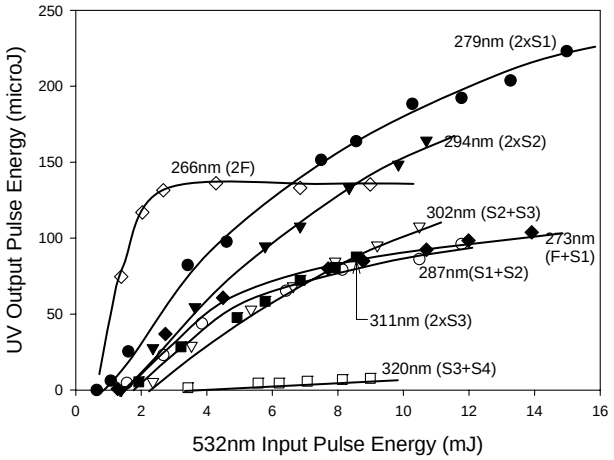


**Fig. 4** Output energy at 10 Hz for each UV wavelength as a function of input energy. (F = fundamental, $S_n$ = nth Stokes.).

Generation of 279 nm output, the second-harmonic of the first Stokes, increases with pump energy in a similar way to that observed for 273 nm but is approximately twice as efficient. The maximum output energy was 223 μJ (ie., 2.2 mW of average output power) at 1.5% conversion efficiency from the pump. The maximum conversion efficiency was 2.4% obtained at ~4 mJ input energy. We have found that the conversion efficiencies for second-harmonics are often notably higher than neighbouring sum-frequency wavelengths both for the 10 Hz and 5 kHz lasers. A summary of the output wavelengths, the maximum energies and conversion efficiencies achieved are summarized in Table III. For examples, the conversion efficiency of 287 nm (the sum frequency of first and second Stokes), is very similar to that obtained for the 273 nm, whereas output at 295 nm (the second harmonic of the second-Stokes) is similar to 279 nm. Though we are yet to investigate this fully, preliminary measurements of temporal pulse shapes indicate that the sum-frequency conversion efficiencies are typically lower in at least part due to reduced temporal overlap of the sub-harmonic components in the BBO crystal. For the longer wavelengths corresponding to nonlinear mixing of 3rd and 4th Stokes, efficiency is limited by the bandwidth of the resonator mirrors (refer also Table I). For example, output at the second harmonic of the third Stokes (311 nm), the lower output efficiency (1.1%) compared to the shorter wavelength second-harmonics can be attributed to substantial loss at the end-mirror for measured to be ~35% at 311 nm. For 320 nm, the efficiency is very low (<0.1%), due to increasing mirror losses at both the end-mirror (65%) and the dichroic output coupler (~10%).

An analysis of the factors that influence conversion efficiency at each wavelength would require consideration of the competing nonlinear sum frequency and Raman cascading processes, as well as the resonator losses at each wavelength. However, the qualitative features of the observed behaviour are consistent with the expected energy transfer amongst the Stokes orders. The decrease in slope-efficiency of wavelengths 273-294 nm for pump energies above 4 mJ is consistent with depletion of the harmonic components by the cascade of energy to higher Stokes orders. By displaying the dispersed output on a screen, we clearly observed 4 Stokes orders when the BBO crystal was angled at phasematching and also when inclined slightly to inhibit UV generation. Though the intensities of the higher Stokes orders were reduced when the BBO was tuned for generating efficient UV output, it is deduced that the Raman process is in close competition with nonlinear sum frequency generation. In contrast, the effect of such cascading on generation of UV output >300nm (corresponding to SF/SH of the 3rd or 4th Stokes wavelengths) is reduced since the threshold for cascading to higher Stokes is raised by increased resonator losses. This is consistent with the more linear output-versus-input energy behaviour observed for wavelengths ≥302 nm.

### *C. Discussion*

The output conversion efficiency demonstrated here has enabled generation of UV output pulse energies the order of 100 μJ. Note that very little attempt to optimise waist sizes, crystal material and length, cavity optics, and thus greater efficiencies are anticipated. However, it was deduced from the results above that the efficiency at many output wavelengths is primarily limited by competition between the nonlinear mixing process and further Raman conversion to higher Stokes orders. Conversion efficiency may thus be improved by increasing the nonlinear coupling coefficient for harmonic mixing, which could be achieved in practice for example by paying additional attention to the beam properties through the BBO crystal in order to ensure that propagation is within the narrow acceptance angle of BBO. Cylindrical focusing geometries, used successfully to improve conversion efficiency in BBO, may also be applied in this case by the use of anamorphic resonator optics. Power loss by cascading to higher Stokes may also be reduced or eliminated by introducing resonator losses at the higher Stokes order by for example careful selection of coatings (though such an approach is most applicable to boosting efficiency at a selected wavelength). By addressing these issues, we believe that widely-tunable UV Raman lasers are likely to be realized with conversion efficiencies more than 10%.

There is also substantial scope to extend the performance of the 532 nm pumped UV Raman lasers detailed above. Though the tuning range demonstrated above already exceeds that capable cerium lasers, the accessible wavelength range may also be extended to further into the UV-A by using mirrors of increased bandwidth.

Finally, it should be noted that output wavelength values and tuning range are dependent on the selected optics and may vary significantly from the two examples of this paper. The use of other Raman materials with a Stokes shift will enable targeting of different output wavelengths, which may be required for applications such as environmental sensing. As mentioned above, the wavelength spacing for KGW can also be changed from 901 $cm^{-1}$ to 768 $cm^{-1}$ by rotating the KGW 90 degrees about the propagation axis. As shown in the following section, the number of wavelength options increases for KGW orientations that provide approximately equal gain on each of its two principal Raman modes.

## V. INCREASED WAVELENGTH OPTIONS WITH BI-MODAL RAMAN MATERIALS

The choice of Raman wavelengths is often limited to the spacing determined by the Raman transition energy. However, many Raman materials have transitions that have energy that shift as a function of orientation (eg., lithium iodate) or have more than one Raman active transition, offering opportunities to generate a large choice of wavelengths. In some crystals, such as the metal double tungstates (which includes KGW), there are two strong Raman modes and the relative gain is varied by rotating about propagation axis (see eg. Fig. 5).

The above wavelength-selectable UV Raman laser was investigated for KGW orientations that enable excitation of two Raman modes simultaneously. This was achieved by rotating the KGW crystal about the propagation axis (ie., the crystal b-axis), thus no change in resonator realignment or configuration was required.

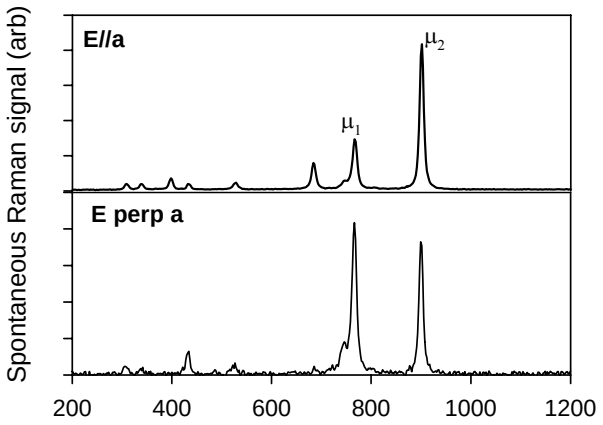


**Fig. 5** Spontaneous Raman spectra for KGW for pump propagation along the $N_p$ axis and polarization aligned parallel and perpendicular to the crystal a-axis. Two strong Raman modes are observed at $h\mu_1$=768cm$^{-1}$ and $h\mu_2$=901cm$^{-1}$.

### *A. Theory – Possible Spectral Combinations*

For 2 Raman modes $\mu_1$ and $\mu_2$, the available Stokes output wavelengths are given by:

$$\nu_{ij} = \nu_f - i\mu_1 - j\mu_2$$

and are depicted in for $n_m \leq 4$ where $n_m$ is the maximum number of Raman modes generated in the medium for a single pump photon. Note that $n_m$ in this case corresponds to the effective Stokes order, ie., the sum of the Stokes orders of both Raman modes. It has practical significance as it is an approximate indicator of the span of output wavelengths and is determined by constraints imposed by the optical resonators such as the bandwidth of mirror and AR coatings as well as the Raman gain. As verified below in the experimental results, the spectrum includes the two separate Stokes spectra ($\nu_f - i\mu_1$ and $\nu_f - j\mu_2$) but may also contain mixtures of the two Raman modes ($\nu_f - i\mu_1 - j\mu_2$, where $i$ and $j$ are nonzero). The maximum number of Stokes wavelengths that can be generated as a function of $n_m$ is thus

$$n_s = \sum_{k=1}^{n_m} (k+1)$$

For example for $n_m = 2$, there are 5 Stokes lines generated at $\nu_f - \mu_1$, $\nu_f - \mu_2$, $\nu_f - \mu_1 - \mu_2$, $\nu_f - 2\mu_2$ and $\nu_f - 2\mu_1$. For $n_m$ values up to 4, which is typically the highest order of Raman excitation observed in our system, the max number of Stokes lines are listed in Table IV. For $n_m$=4, the number of possible SF/SH wavelengths increases more than 5-fold for a material with 2 Raman modes.

The additional Stokes frequencies available for $n_m > 1$ leads to a rapid expansion of the output options when generating additional harmonics via nonlinear mixing. Though generation of higher order Stokes lines is achieved via a stepwise cascade process, good temporal overlap between each Stokes order is generally achieved allowing conversion to other wavelength regions via second-harmonic, sum and difference frequency generation.

**Table IV** The number of Stokes lines and harmonic wavelengths that can be generated as a function of $n_m$.

| **Modes excited $n_m$** | **Stokes lines $n_s$** | | **Number SFG/SHG wavelengths $n_{SFG}$** | | **Number DFG wavelengths $n_{DFG}$** | |
|---|---|---|---|---|---|---|
| | 1 mode | 2 modes | 1 mode | 2 modes | 1 mode | 2 modes |
| 1 | 1 | 2 | 2 | 6 | 1 | 3 |
| 2 | 2 | 5 | 4 | 15 | 2 | 9 |
| 3 | 3 | 9 | 6 | 28 | 3 | 17 |
| 4 | 4 | 14 | 8 | 45 | 4 | 28 |

For sum frequency mixing and second harmonic generation, the possible output frequencies are the various combinations of $\nu_{ij} + \nu_{kl}$ where integers $i$, $j$, $k$ and $l$ are less than or equal to $n_m$. For sum frequency mixing it easily shown that there are up to

$$n_{SFG} = \sum_{i=0}^{n_m} (4i+1)$$

unique SF/SH wavelengths available. Note that the number of wavelengths also increases for infrared generation by difference frequency mixing, and the number of unique DF wavelengths $\nu_{ij} - \nu_{kl}$ is:

$$n_{DFG} = -1 + \sum_{i=1}^{n_m} 2(i+1)$$

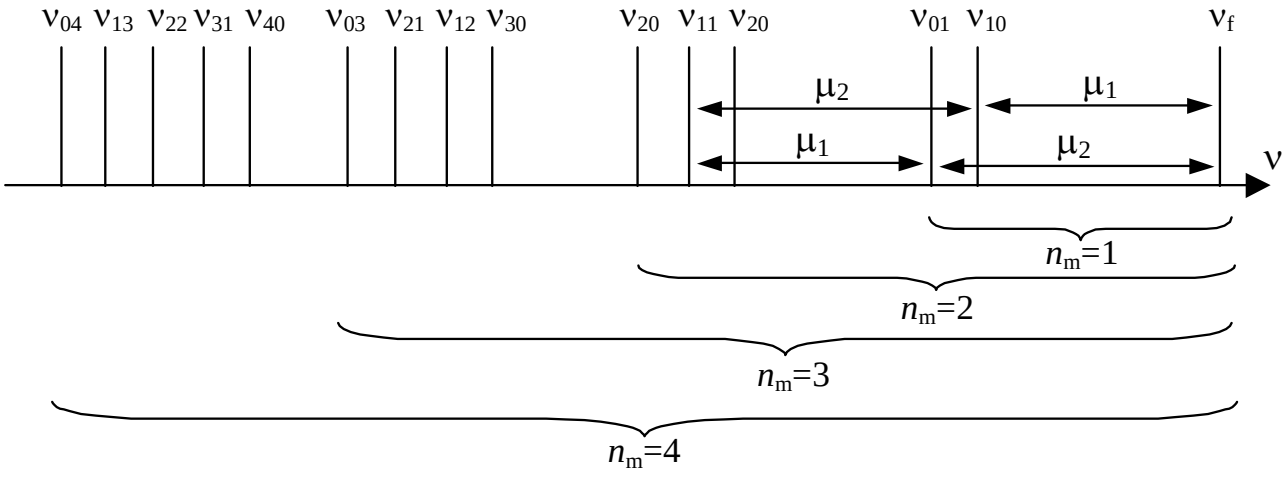


**Fig. 6** Stokes spectra for Raman lasers with 1 and 2 active Raman modes shown for $n_m \leq 4$.

Table IV shows that the number of SF/SH and DF wavelengths available increases up to 45 and 28 respectively for $n_m = 4$.

### *B. Results - Visible Stokes Generation*

The cascade of the pump beam into the various Stokes orders was investigated as a function of KGW rotation angle by measuring the visible output spectrum for the Raman laser of Fig. 3 with the BBO crystal angle displaced to ensure negligible conversion to the ultraviolet. For the nominal pump energies of ~2 mJ, the visible Stokes spectrum varies with rotation angle as shown in Fig. 7. As $\nu_f - (i-1)\mu_1 - j\mu_2$ where $j \leq 1$ and $i + j \leq 5$. The appearance of the $\mu_2$ mode is consistent with the similar gain on this transition for *E* perp a-axis (ie., $\phi = 0$) observed in the spontaneous Raman spectrum of Fig. 5. The fact that only a maximum of only 1 $\mu_2$ mode can be excited per pump photon, compared to up to 5 for $\mu_1$, suggests the Raman gain coefficient for $\phi = \sim 20°$ is slightly higher for $\mu_1$.

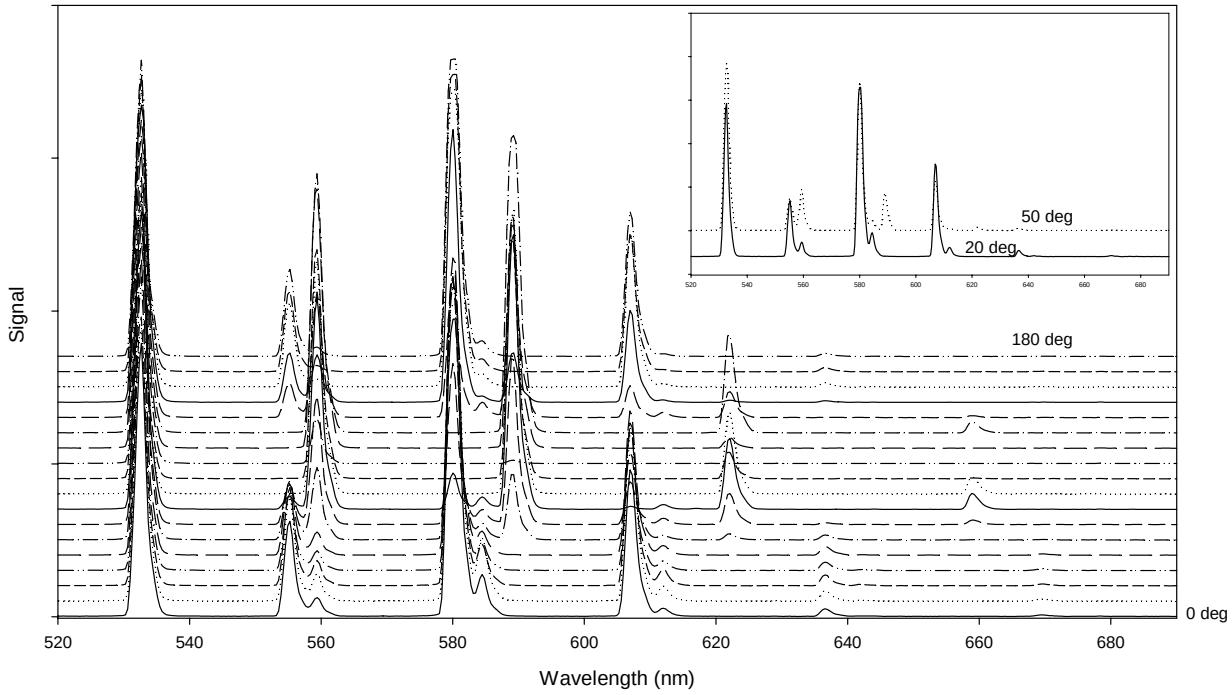


**Fig. 7** Visible output spectra of the Raman laser as a function of the rotation angle f about the propagation axis. The rotation angle ϕ=0 deg corresponds to crystal aligned perpendicularly to the a-axis.

**Table V** Visible Stokes orders observed in the Raman laser for three KGW rotation angles [12].

| Raman modes excited per output Stokes photon | | Stokes wave-length (nm) | KGW rotation angle ϕ | | |
|---|---|---|---|---|---|
| | | | 20° | 50° | 110° |
| $\mu_1$ | $\mu_2$ | | Observed Stokes lines | | |
| 1 | 0 | 554.7 | ✓ | ✓ | - |
| 0 | 1 | 558.9 | ✓ | ✓ | ✓ |
| 2 | 0 | 579.4 | ✓ | ✓ | - |
| 1 | 1 | 583.9 | ✓ | ✓ | - |
| 0 | 2 | 588.5 | - | ✓ | ✓ |
| 3 | 0 | 606.4 | ✓ | ✓ | - |
| 2 | 1 | 611.3 | ✓ | ✓ | - |
| 1 | 2 | 616.4 | - | ✓ | - |
| 0 | 3 | 621.5 | - | ✓ | ✓ |
| 4 | 0 | 636.0 | ✓ | ✓ | - |
| 3 | 1 | 641.4 | ✓ | - | - |
| 0 | 4 | 658.4 | - | - | ✓ |
| 5 | 0 | 668.6 | ✓ | - | - |
| 4 | 1 | 674.6 | ✓ | - | - |

When rotating the KGW for $\phi = 50 - 70°$ and 140-150°, we observe Raman lines that include those seen for ϕ=0-40° as well as Stokes lines corresponding to the second and third orders of the $\mu_2$ Raman line (refer also Fig. 7). It is noted, however, these additional lines are at the expense of the higher-order lines at wavelengths >640 nm. Ten wavelengths are observed having wavelengths that correspond to $\nu_f - (i-1)\mu_1 - j\mu_2$ where $j \le 3$ and $i + j \le 4$. We deduce that at these orientate on angles there is approximately balanced gain at both $\mu_1$ and $\mu_2$ Raman modes.

It should be noted that the resonator is optimally designed for visible output and as a result the conversion efficiency of the pump to the Stokes output is low (<10%). The output coupling at visible wavelengths is <2%, which is commensurate with the combined losses at on the other cavity optics. Moreover, there are two output beams due to reflections of both counter-propagating fields on the output coupler. However, it is straightforward to optimise the Raman laser for efficient Stokes generation at the above wavelengths by removing the BBO and UV dichroic and replacing an end-mirror with an output coupler (with transmission >10% for example) at the selected output wavelength(s).

### *C. Results – Switchable Ultraviolet output*

Sum frequency and second harmonic outputs of the laser were determined as a function of the BBO rotation angle in the phase matching plane. We find that the available UV wavelengths depends on the KGW rotation angle as expected according to the visible Stokes sub-harmonics oscillating in the resonator (as listed in Table V).

For ϕ =20°, 23 lines were observed in the range 266 to 321nm as listed in Table VI. The strengths of the output harmonics vary according to the strength of the Stokes sub-harmonics and also the temporal pulse overlap in the case of the sum frequencies. As a general rule the strongest lines are the ones that are second-harmonics. Also, the stronger lines tend to consist of only 1 Raman mode (ie., for no Raman mode mixing) or at most correspond to excitation of one quantum of the secondary Raman mode. Note that the Raman laser is able to also generate some closely spaced lines simultaneously eg, 292.0 nm and 293.1nm.

**Table VI** Output wavelengths for the intracavity doubled Raman laser.

| Raman modes per UV photon | | Wave-length (nm) | Expected Assign-ment* | KGW rotation angle ϕ (deg) | | |
|---|---|---|---|---|---|---|
| $\mu_1$ | $\mu_2$ | | | 20 | 50 | 110 |
| 0 | 0 | 266.0 | $\nu_f$ x2 | ✓ | ✓ | ✓ |
| 1 | 0 | 271.6 | $\nu_f + \nu_{10}$ | ✓ | ✓ | |
| 0 | 1 | 272.6 | $\nu_f + \nu_{01}$ | ✓ | ✓ | ✓ |
| 2 | 0 | 277.4 | $\nu_{10}$x2 | ✓ | ✓ | |
| 1 | 1 | 278.4 | $\nu_{10}+\nu_{01}$ | ✓ | ✓ | |
| 0 | 2 | 279.4 | $\nu_{01}$x2 | ✓ | ✓ | ✓ |
| 3 | 0 | 283.4 | $\nu_{10}+\nu_{20}$ | ✓ | ✓ | |
| 2 | 1 | 284.5 | $\nu_{01}+\nu_{20}$ | ✓ | ✓ | |
| 1 | 2 | 285.6 | $\nu_{11}+\nu_{01}$ | ✓ | ✓ | |
| 0 | 3 | 286.7 | $\nu_{01}+\nu_{02}$ | | | ✓ |
| 4 | 0 | 289.7 | $\nu_{20}$x2 | ✓ | ✓ | |
| 3 | 1 | 290.8 | $\nu_{21}+\nu_{01}$ | ✓ | | |
| 2 | 2 | 292.0 | $\nu_{11}$x2 | ✓ | ✓ | |
| 1 | 3 | 293.1 | $\nu_{11}+\nu_{02}$ | | ✓ | |
| 0 | 4 | 294.4 | $\nu_{02}$x2 | | | ✓ |
| 5 | 0 | 296.3 | $\nu_{20}+\nu_{30}$ | ✓ | ✓ | |
| 4 | 1 | 297.5 | $\nu_{30}+\nu_{11}$ | ✓ | ✓ | |
| 3 | 2 | 298.7 | $\nu_{21}+\nu_{11}$ | ✓ | ✓ | |
| 2 | 3 | 299.9 | $\nu_{11}+\nu_{12}$ | | ✓ | |
| 0 | 5 | 302.3 | $\nu_{02}+\nu_{03}$ | | | ✓ |
| 6 | 0 | 303.2 | $\nu_{30}$ x2 | ✓ | ✓ | |
| 5 | 1 | 304.4 | $\nu_{21}+\nu_{30}$ | ✓ | | |
| 4 | 2 | 305.7 | $\nu_{21}$x2 | ✓ | ✓ | |
| 0 | 6 | 310.8 | $\nu_{03}$x2 | | | ✓ |
| 7 | 0 | 310.4 | $\nu_{30}+\nu_{40}$ | ✓ | ✓ | |
| 6 | 1 | 311.7 | $\nu_{21}+\nu_{40}$ | ✓ | | |
| 5 | 2 | 313.0 | $\nu_{21}+\nu_{31}$ | ✓ | | |
| 8 | 0 | 318.0 | $\nu_{40}$x2 | ✓ | | |
| 7 | 1 | 319.3 | $\nu_{40}+\nu_{31}$ | ✓ | | |
| 0 | 7 | 319.7 | $\nu_{04}+\nu_{03}$ | | | ✓ |
| 6 | 2 | 320.7 | $\nu_{31}$x2 | ✓ | | |

*Multiple assignments are possible and output may comprise of more than one sum frequency and second harmonic. The most significant contributor is listed as deduced from the observed strength of intracavity fields.

For ϕ =50°, a similar number of output lines are observed but the flow of pump energy can directed to a different array of Stokes orders providing a different choice of selectable UV output lines. 20 lines were observed in the range 266 to 321nm with UV output

wavelengths involving second and third order excitation of the $\mu_2$ Raman mode.

The results in Table VI show that up to 31 wavelengths in the range 271 – 321nm can be selected by appropriate orientation of the BBO and KGW Raman crystal. The large wavelength choice and tuning range is well suited for diverse range of applications including biosensing, tactical communications, environmental sensing and in medicine.

## VI. CONCLUSION

Wavelength selectable Raman lasers have been demonstrated for output spanning the 532-650nm and 266-320nm regions. These systems hold promise for satisfying the requirements of applications requiring broadly tunable and narrow linewidth output in the visible and ultraviolet. The concept may also form the basis of novel infrared sources through the use of intracavity difference frequency generation.

**Acknowledgements**

The author wishes like to thank Prof. Jim Piper and Dr Helen Pask for their support and expert advice during this work.

## VII. REFERENCES

**[1]** T. T. Basiev and R. C. Powell, "Solid-state Raman lasers," in Handbook of Laser Technology and Applications, C. E. Webb et al., Ed. London, U.K.: Inst. Phys., , ch. B1.7, pp. 469–497, 2003.

**[2]** H. M. Pask, "The design and operation of solid-state Raman lasers," *Progress Quantum Electron.*, Vol. 27, pp1–56, 2003.

**[3]** P. Cerny, H. Jelinkova, P. G. Zverev, and T. T. Basiev, "Solid state lasers with Raman frequency conversion," Progress Quantum Electron., vol. 28, pp113–143, 2004.

**[4]** H. M. Pask and J. A. Piper, "Crystalline Raman Lasers," *IEEE J. Sel. Topics in Quantum Electron.*, Vol. 13 , p692-704, 2007.

**[5]** R. P. Mildren, H. M. Pask, and J. A. Piper, "High-Efficiency Raman converter generating 1.5W of red-orange output," Advanced Solid State Photonics, Jan 29-Feb 1, Lake Tahoe USA, Paper MC3, 2006.

**[6]** E. O. Ammann, "Simultaneous stimulated Raman scattering and optical frequency mixing in lithium iodate," *Appl. Phys. Lett.*, Vol. 34, pp838-846 1979.

**[7]** I. V. Mochalov, "Laser and nonlinear properties of the potassium gadolinium tungstate laser crystal $KGd(WO_4)_2:Nd^{3+}$ (KGW:Nd)", *Opt. Eng*., Vol. 36, PP. 1660-9, 1997.

**[8]** R. P. Mildren, H. M. Pask, H. Ogilvy, and J. A. Piper, "Efficient, all-solid-state, Raman laser in the yellow, orange and red," "Discretely tunable, all-solid-state laser in the green, yellow and red," Opt. Lett., Vol. 30, pp1500-2, 2005.

**[9]** D. W. Coutts and A. J. S. McGonigle, "Cerium-Doped Fluoride Lasers," *IEEE J. Quantum Electron.*, Vol. 40, pp1430, 2004.

**[10]** See for example J. Hecht, "Semiconductor sources advance deeper into the ultraviolet," in Laser Focus World (Pennwell, 2005), P. 95.

**[11]** V. V. Ermolenkov, V. A. Lisinetskii. Ya. I. Mishkel, A. S. Grabchikov, A. P. Chaikovskii, and V.A. Orlovich, "A radiation source based on a solid-state Raman laser for diagnosing tropospheric ozone," *J. Opt. Technol.*, Vol. 72, P. 32, 2005.

**[12]** R. P. Mildren, M. Convery, H. M. Pask, J. A. Piper, and T. Mckay, "Efficient, all-solid-state, Raman laser in the yellow, orange and red", *Opt. Express*, Vol. 12, pp785-790, 2004.